ULTRABROADBAND SOLID-STATE LASERS IN TRACE GAS SENSING

EVGENI SOROKIN*
Photonics Institute, Technische Universitä Wien, Gusshausstr. 27/387, A-1040 Vienna, Austria

Abstract. Application of ultrabroadband Cr^{2+}-doped mid-infrared lasers to sensitive molecular spectroscopy in the 2–3 μm wavelength range is demonstrated using two different techniques: scanning photoacoustic spectroscopy and intracavity absorption spectroscopy. It is shown, that the broad gain bandwidth is a crucial parameter, allowing multicomponent analysis and extreme sensitivity down to 10^{-5} mbar of partial pressure (H_2O vapor). A number of previously unknown combination bands in CO_2, N_2O and C_2H_2 have been observed. The demonstrated spectral resolution reached 0.1 cm^{-1} for the photoacoustic technique, which is sufficient for multicomponent analysis. For intracavity technique the demonstrated resolution was 0.006 cm^{-1}, which is below the Doppler-limited linewidth. The laser devices are application-ready and allow directly diode-pumped self-contained implementation.

1. Introduction

The room-temperature solid-state lasers have made a significant advance into the mid-IR domain. In addition to long-known rare-earth ion based crystalline media, there exist nowadays also the broadband transition-metal ion doped crystals. These lasers matured from demonstration objects to versatile application-ready tools, notably the optically pumped Cr^{2+}-doped II-VI semiconductors. In this chapter, the recent applications of Cr^{2+}:ZnSe and Cr^{2+}:ZnS in trace gas sensing will be reviewed.

In order to fully exploit the advantages of mid-infrared lasers in applications, they should be used in a different way, as compared to shorter-wavelength lasers, e.g. in the visible. The scaling rules of the nonlinear-optical interactions favor in most cases shorter wavelengths, this is especially true for scattering-based techniques, like Raman, CARS etc. The exact value of the laser wavelength in such techniques does not play immediate role, since it is only the frequency shift that matters. Much more important is the fact, that scattering efficiency scales strongly with inverse wavelength, so that visible lasers are by far more useful for these types of measurement.

* e.sorokin@tuwien.ac.at

M. Ebrahim-Zadeh and I.T. Sorokina (eds.), Mid-Infrared Coherent Sources and Applications, 557–574.

To the contrary, for direct absorption measurements, the light source should come as close as possible to the transition wavelengths. In case of the molecular absorption, like e.g. in gases, the fundamental transitions lie in the mid-infrared from 2.3 to about 10 μm. While it is possible to interact also with obertones or combination bands, the absorption cross-section for such bands rapidly decreases with wavelength. The long-wavelength lasers, approaching the fundamental vibrations of molecules and solids are much better candidates for such measurements. For this reason the first applications tackled by the Cr^{2+}-based lasers lie within the field of trace gas sensing and ultrasensitive spectroscopy described in this chapter. The availability of the possibly broadest gain bandwidth is another critical issue for spectroscopic and sensing applications, as will be shown below.

2. Cr^{2+}-based mid-IR lasers

From this point of view, the Cr^{2+}:ZnSe and other Cr^{2+}-chalcogenide laser materials appear promising: they offer very broad gain bands, centered in the mid-IR regions between 2 and 3.5 μm [1]. Additionally, they operate at room temperature and can be pumped with available solid-state, fiber, and diode lasers. The key specific properties of the lasers, based on Cr^{2+}-doped II-VI compounds are as follows:

- room-temperature and directly diode-pumped operation;
- continuous tuning over an extremely broad wavelength range (e.g. 2000–3100 nm for continuous-wave Cr:ZnSe [2]);
- average output power >1 W in continuous-wave operation;
- average power >10 W in pulse regime at kHz repetition rate;
- extremely narrowband operation (down to single-frequency), and
- modelocked ultrashort-pulsed operation.

For more information the reader is referred to the chapter II.3 in this volume.

It should be noted, that there exist competing technologies for obtaining radiation with high degree of transversal coherence in this wavelength range. Notably, the semiconductor lasers have by now made a tremendous advances towards the mid-IR, reaching 3.26 μm [3]. Other successful techniques are based on nonlinear-optical methods and include optical parametric oscillators (OPO) and difference frequency generators (DFG). In comparison with these techniques solid-state lasers offer convenient ultraboradband tuning at high average power power. From semiconductor lasers, they are distinguished by orders of magnitude broader tuning range, and from nonlinear-optical techniques by much lower cost and complexity. One of the spectroscopic techniques, that especially benefits from high output power is photoacoustic spectroscopy. The solid-state lasers can also

be operated in unique regimes, such as femtosecond or non-stationary operation. The latter can be used for ultrasensitive intracavity absorption spectroscopy, as will be discussed below.

In the experiments described further in this chapter, we have been using laser setups, all being built according to the generic scheme, shown in Fig. 1.

This scheme follows the astigmatically compensated four-mirror design, featuring maximum of flexibility: free choice of cavity length and beam size inside the crystal, and two arms with collimated beams for placing the intracavity elements and output couplers. For broadest tuning range it is important, that all surfaces, e.g. the active element itself, prisms, etc. use only Brewster-oriented surfaces. Without the tuning elements the main wavelength-dependent losses originate from the mirror coatings and reabsorption in the crystal at the blue side of the gain spectrum.

For experiments described in this chapter, we were using different kinds of mirrors, as shown in Fig. 2. It is important to note, that the gain bandwidth of the

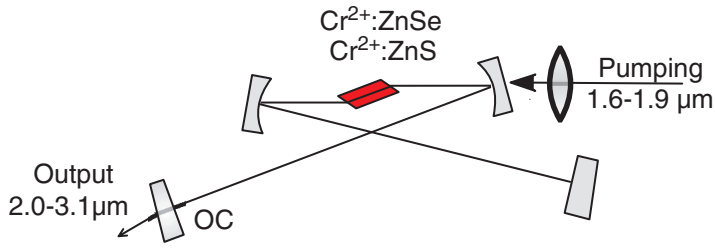

Figure 1. The generic four-mirror cavity design for Cr:ZnSe and Cr:ZnS lasers. The mirror radii of curvature varied from 75 to 150 mm, and pump lens focusing distance from 40 to 100 mm. All mirrors except the output coupler (OC) are dichroic high reflectors.

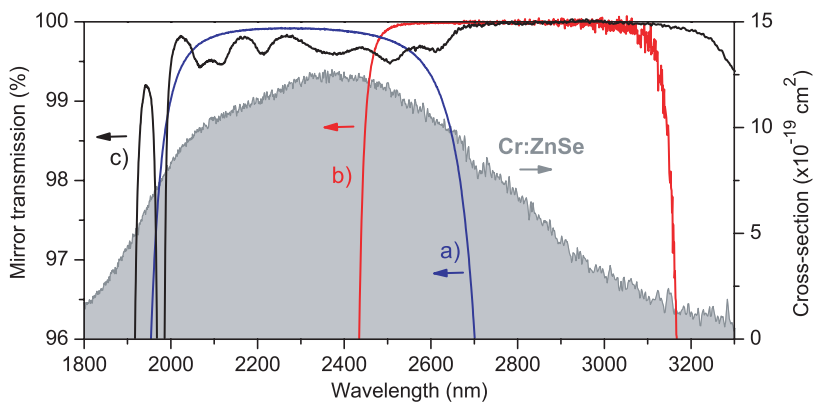

Figure 2. Reflection curves of the high-reflection mirror coatings. The coatings a) and b) use the high index contrast dielectric layers and follow the conventional quarterwave-stack design. The coating c) uses the 51-layer chirped-mirror design, allowing to cover the entire operation range with a single set of mirror, at the expense of increased losses. All coatings are dichroic, with low reflectivity in the 1.6–1.9 μm range for pump radiation. Filled area shows the gain cross-section of Cr:ZnSe.

Cr^{2+}-based active media is so broad, that one would need at least two different mirror sets to cover it, if the coating are made using the traditional quarterwave stack design and dielectric materials with the highest index contrast. To cover the whole gain range of the Cr:ZnSe or Cr:ZnS laser with a single mirror is a very challenging task, requiring the special broadband mirror designs. With such mirrors, designed according to the "chirped mirror" technique [4] it was possible to operate the laser in almost the entire tuning range (Fig. 4), although losses in these mirrors are far from optimal (Fig. 2c).

3. Trace gas analysis in the atmosphere

The monitoring and analysis of gases at low concentration has become an essential environmental, medical, industrial, and chemical issue. Numerous techniques and instruments have been invented, reaching extremes in sensitivity for certain components. The optical techniques possess some important advantages, e.g. they can be performed without intrusion, in real time, and on a number of components simultaneously, etc.

One of the optical techniques based on direct absorption spectroscopy is the photoacoustic (PA) spectroscopy. It requires a tunable narrow linewidth light source and a detection scheme based on photoacoustic effect, e.e. generation of sound waves in the medium by nonradiative decay of molecules, excited by modulated radiation. Being specimen- and wavelength-independent, the PA detection scheme is quite universal. This property is especially important if the measurement is supposed to include different gases, as it is normally the case in typical applications.

The PA signal is directly proportional to the absorption cross-section $\sigma(\lambda)$ and the power of the exciting radiation [5, 6]:

$$S(\lambda) = q\sigma(\lambda)NP(\lambda), \tag{1}$$

where N is the concentration of the molecules, and $P(\lambda)$ the wavelength-dependent power of the exciting beam. The sensitivity coefficient q in the equatuion (1) depends on the construction of the cell and microphones, and can be further enhanced by utilizing the acoustic or mechanical resonance. The resonance signal enhancement is typically of the order of $\sim$10–100 for multi-microphone cells with acoustic resonance but can reach values up to $\sim 10^4$–10^5 using the electromechanical resonances [7]. The equation shows another advantage of the photoacoustic technique. In comparison with many other absorption measurement schemes, where the absorption signal is derived as a ratio between the absorbing and non-absorbing (baseline) spectra, the signal $S(\lambda)$ is directly proportional to the absorption of the specimen. When the measurement is aimed at detecting the very low absorption, this property strongly lowers the

necessary signal-to-noise figure, allowing measurement of absorption of down to $10^{-8}\,\mathrm{cm}^{-1}\mathrm{Hz}^{-1/2}$ despite the much lower sensitivity of the PA technique as compared to, e.g., optical detectors.

To fully exploit this advantages of the PA scheme, the excitation laser source should demonstrate broad tunability in the wavelength range of potential specimens, sufficiently narrow oscillation linewidth for good selectivity, and high output power for more sensitivity. Currently available alternatives include systems, based on nonlinear optical conversion techniques and include optical parametric oscillators, difference frequency generators, and tunable semiconductor lasers [6, 8, 9]. The latter are probably most user-friendly, but so far they provide only relatively narrow tuning ranges, making every setup suitable to just one-two species. The tunable broadband solid-state laser, directly covering thousands of wavenumbers provide a really multicomponent ability.

The main absorption features of many relevant gases lie in the midinfrared (2–15 μm) region with overtones and combination vibrational-rotational bands in the near-IR (0.8–2 μm) spectral range. The atmospheric window between 2–5 μm is especially interesting, because it is characterized by the presence of the strong fundamental vibrational absorption lines of atmospheric constituents, vapors and other gases. Those include water vapour (H_2O), filling the whole range between 2.4 and 3 μm with maximum around 2.7 μm, carbon monoxide (CO) with strong features around 2.3–2.4 μm, carbon dioxide (CO_2) absorbing around 2.7–2.8 μm, nitrous oxide (N_2O), having several absorption features all through the 2–4 μm range, as well as many other species. In what follows, the application of the tunable Cr^{2+}:ZnSe laser source to PA-based trace gas measurement is described.

The measurement scheme is shown in Fig. 3. The laser source was the tunable Cr^{2+}:ZnSe laser, as described in the previous section, pumped by an Er^{3+}-fibre laser at 1607 nm. In continuous-wave operation, this type of active medium acts

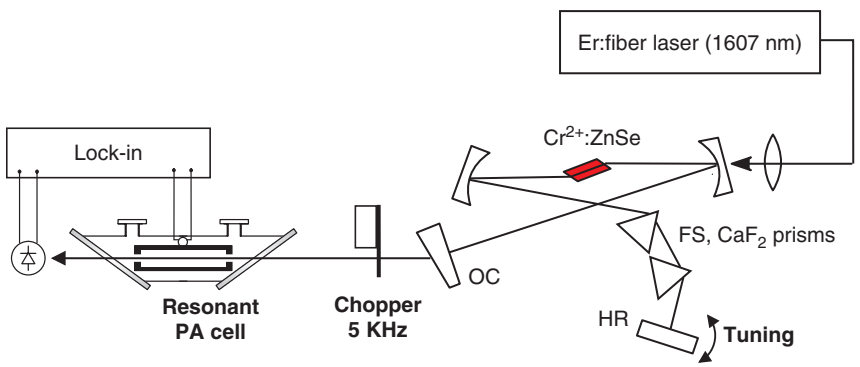

Figure 3. Experimental setup for the photoacoustic measurements. The resonator section of the PA cell had opening diameter of 3 mm and resonance enhancement factor of 4.2 at 5.7 kHz [11].

as a homogeneously broadened one [10] so that narrowband tunable operation can be achieved without efficiency penalty. This allows higher output power, which translates into better signal-to-noise ratio according to the expression (1).

The tuning has been achieved by a tandem of prisms by rotating the end mirror. Depending on the required spectral resolution and spectral region, CaF_2 or dry fused silica prisms have been used. The relative acceptance bandwidth (full-width at half-maximum) of the tuning arrangement in this case is given by the formula

$$\frac{\Delta\lambda}{\lambda} = \frac{1}{8\pi w_0}\left(\frac{dn}{d\lambda}\right)^{-1}, \tag{2}$$

where w_0 is the beam waist radius. The final oscillation linewidth also depends on the cavity arrangement, saturation, and loss level, but in any case it scales with the acceptance bandwidth, i.e. inversely proportional to the prism material dispersion. Table 1 gives dispersion data for some common materials. Fused silica provides the highest dispersion over the whole tuning range, but it suffers OH-related losses beyond 2.5 μm. This is a common problem for many oxide materials, which should be substituted by fluorides or chalcogenides at longer wavelengths. Interestingly, we found that ZnSe does not have any advantages over CaF_2 beyond 2.5 μm, despite its much higher refractive index.

In the experiments, both dry fused silica and calcium fluoride for tuning and PA measurements. With a single broadband mirror set, a wavelength range between 2000–2937 nm (3400–5000 cm^{-1}) can be covered (Fig. 4). With special infrared optics, it is possible to extend the tuning range to 3100 nm. (Fig. 4).

The typical experimental results are presented in Fig. 5. Using the same source it was possible to perform measurements from 2.3 μm to 2.9 μm. The laser output power of 100–500 mW is orders of magnitude higher than the powers achieved with difference frequency generation in the same wavelength range. This allows sensitive measurement using even the relatively weak absorption lines in the spectrum. Using the certified gas mixtures, one can calibrate the sensitivity of the whole setup and perform quantitative measurements [11]. The minimum detectable absorbance at a power level of 300 mW was 1.6×10^{-5}. The resulting

TABLE 1. Material dispersion $dn/d\lambda$ ($\times 10^{-6}$ nm^{-1}) for some common prism materials: zinc selenide, calcium fluoride, and fused silica. The wavelengths correspond to the tuning range of the the Cr:ZnSe laser.

Material	$\lambda = 2100$ nm	$\lambda = 2500$ nm	$\lambda = 3000$ nm
ZnSe	−12.3	−7.9	−5.4
CaF_2	−5.23	−6.0	−7.05
SiO_2	−15.4	−18.7	−23.7

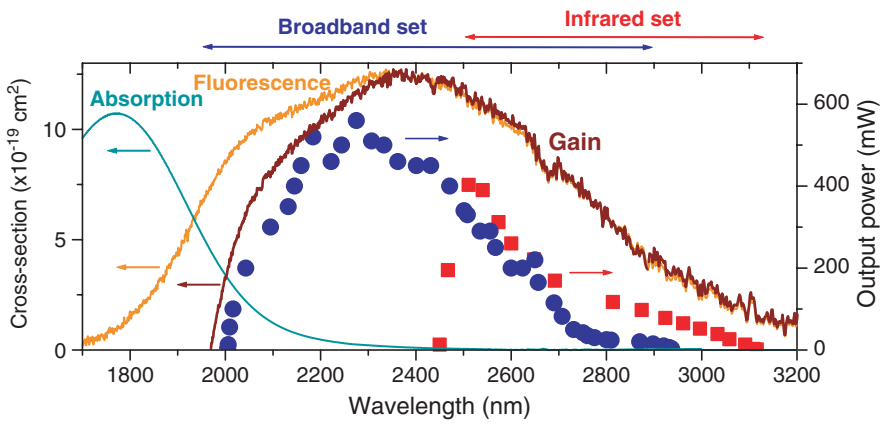

Figure 4. Continuous-wave tuning of a Cr:ZnSe laser, using a broadband mirror set (circles) and an infrared mirror set (squares). The effective gain curve is computed from the fluorescence and absorption cross-sections at real ion concentration N_t and threshold inversion n_{th} [2].

minimum detectable concentrations for a number of gases are plotted in Fig. 6, [11, 12]. For many important molecules the detection limit lies well in the ppb (part-per-billion) region.

The linewidth of the laser is also an important factor, as it defines the selectivity of the technique. It was measured using the gas lines themselves and was found to be $\sim$0.2 cm^{-1} with fused silica prisms (Fig. 5c) and $\sim$1.2 cm^{-1} with CaF_2 prisms Fig. 5d), due to their lower dispersion [12]. This linewidth is still dominated by the thermal and mechanical instability of the used laser setup, because the short-term linewidth in the comparable setup was measured to be less than 0.02 cm^{-1} [1]. Nevertheless, for atmospheric measurements the resolution of the current setup with CaF_2 prisms is in most cases sufficient for measurements of vibrational-rotational absorption bands, and fused-silica prisms allow resolution of single absorption lines.

4. Intracavity laser spectroscopy

Another method of ultrasensitive spectroscopic absorption measurements, where the gain bandwidth plays a crucial role, is the time-resolved intracavity laser spectroscopy (ICLAS) [13]. The principle of ICLAS can be summarized as follows: after a fast switching on of the pumping, the broadband laser will initially start its oscillation from the amplified spontaneous emission, which is effectively a gain spectrum of the active medium. Along with the settlement of the continuous-wave operation, the oscillation spectrum will implode to its stationary value. During this time any narrowband loss inside the cavity (e.g. an absorption line in the air) will appear as a dip in the spectrum. It can be shown, that the form and the depth

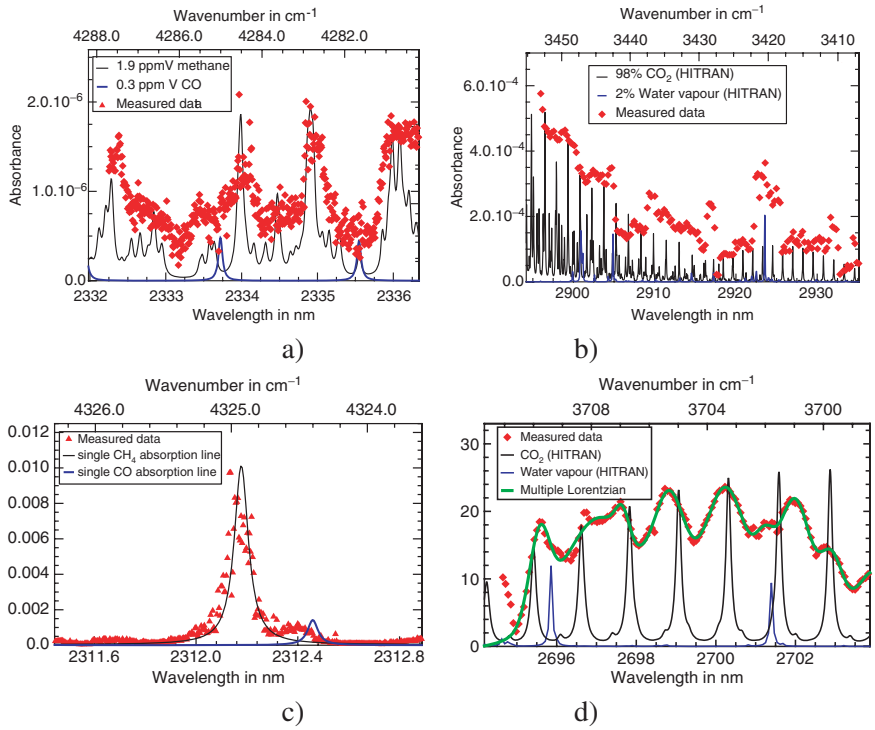

Figure 5. Gas absorption spectra using the tunable Cr:ZnSe laser.
a) Methane and carbon monoxide in air (1 bar) around 2.3 μm [11].
b) Overview scan of CO_2 (1 bar, contaminated with 2% water) around 2.9 μm [12].
c) Methane (500 mbar), single narrow line for resolution estimation [11].
d) CO_2 (1 bar, contaminated with 2% water) around 2.7 μm [12].
All measurements performed at room temperature. Spectra a) and c) recorded with fused silica tuning prisms, spectra b) and d) used calcium fluoride prisms.

of the absorption line relative to the broadband spectrum follows the exponential Bouguer-Beer law with an effective propagation distance equal to $l_{\text{eff}} = c(t - t_0)$, where t_0 denotes the onset of laser oscillation.

In properly designed low-loss lasers, the spectrum collapse may take tens and hundreds of microseconds, resulting in effective absorption lengths of tens and even hundreds of kilometers, allowing measurement of absorption as small as 10^{-9} cm^{-1} and better. This explains the enormous potential of the ICLAS measurement for detection of weak narrowband absorbers. At the same time, the initially broad spectrum continues to narrow during the laser evolution, so that the maximum effective absorption length can be reached only near the gain maximum. More precisely, it can be shown that the laser bandwidth at a time t after the onset of oscillation follows the rule [13]

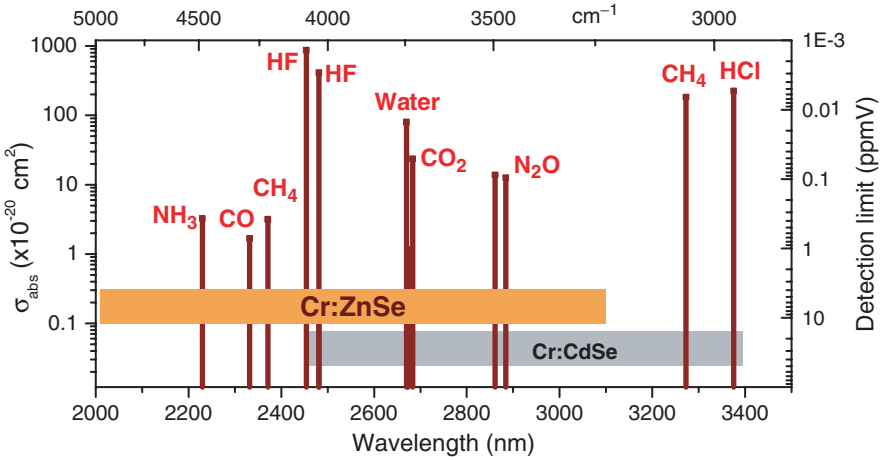

Figure 6. Minimum detectable concentrations for a number of gases using the photoacoustic registration. The horizontal bars show the tuning ranges of Cr:ZnSe and Cr:CdSe lasers [2].

$$\Delta\lambda \propto \Delta\lambda_0 \cdot \sqrt{\frac{\tau_c}{(t - t_0)}}, \tag{3}$$

i.e. it is proportional to the initial bandwidth $\Delta\lambda_0$ of the gain spectrum. In the expression (3) τ_c is the lifetime of the photon in the resonator, depending on the resonator round-trip time T_R and the round-trip loss L: $\tau_c = T_R/L$. The optimal laser for the ICLAS experiment should thus exhibit low loss and have possibly long resonator, since the effective absorption path is proportional to the length of the resonator and inversely scales with losses. Reversing the relation (3) makes also clear, that the laser bandwidth is an even more important factor: for a given final bandwidth the effective absorption path length scales *quadratically* with the initial bandwidth: $l_{\text{eff}} = c(t - t_0) \propto \Delta\lambda_0^2$. The material bandwidth becomes thus a most crucial parameter in the intracavity spectroscopy. For detailed description of ICLAS using the solid-state lasers the reader is referred to Refs. [13–15].

With respect to the above discussion, Cr^{2+}:ZnSe and Cr^{2+}:ZnS lasers fit extremely well for the ICLAS spectroscopy: the lasers allow convenient operation at room temperature in a very interesting wavelength range, and possess the broadest gain bandwidth of all known solid-state laser materials [10]. The gain peaks of the two lasers are shifted by about 100 nm (Fig. 7), so that they can be seen as complementary in coverage of the 2.2–2.7 μm region. These media also represent a much broader family of Cr^{2+}-doped II-VI materials with a potential of extending the wavelength coverage to and beyond 3 μm [1, 10].

Only a few experiments with ICLAS using broadband sources in the infrared were performed: atmospheric spectra were obtained in the 2636–2640 nm region using the KCl:Li F_A(II) color center laser [16], in the 2035–2055 nm region using

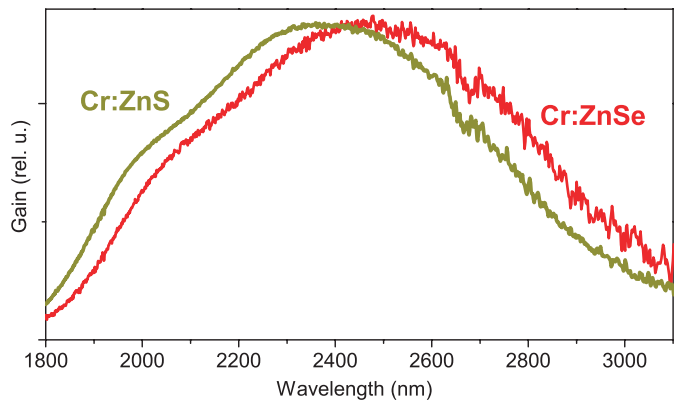

Figure 7. Comparison of the normalized gain spectra of Cr:ZnSe and Cr:ZnS laser materials.

the Co:MgF_2 laser [17], and in the 1770–1950 nm region using the Tm-doped fiber laser [18]. Quite recently, the Cr:ZnSe laser has been used for the intracavity absorption experiment in the 2410–2460 nm region [19], and a Cr^{4+}:YAG laser has been applied in the 1350–1610 nm range [20].

However, the extreme sensitivity of the intracavity spectroscopy becomes a problem, if it is used in the infrared region, were air constituents possess fundamental and combination absorption lines. As a result, in most of the above quoted experiments the spectra were completely oversaturated by the atmosphere, predominantly water vapor and CO_2. Equally, even the slightest back-reflection from any surface inside or outside of the resonator creates a weak loss modulation in form of parasitic Fabry-Perot resonance, which act in the same way as a comb of absorption lines. The laser must therefore be carefully optimized with respect to spurious reflections and contain no plan-parallel mirror substrates. Equally detrimental could be residual birefringence in the laser material, when the active element might acts as a shallow Lyot filter, also resulting in spectral loss modulation.

In order to make use of the full ICLAS sensitivity in the mid-IR range, we have put the Cr:ZnSe (Cr:ZnS) laser setup into the sealed chamber [21–23]. With an Er:fiber laser pumping, the pumping head was positioned outside the chamber (Fig. 8). For sufficiently fast (few microseconds) turning on of the pump, an acousto-optical modulator was used. The box was then evacuated and filled with a gas of interest at pressures between 0.1–70 mbar, to avoid the collisional broadening. The output of the laser from the output coupler with an average power of tens of mW is atttenuated and examined outside of the evacuated chamber using the Fourier-transform spectrometer in the step-scan mode [24]. In this regime, the complete time sequence is recorded at every position of the FT interferometer. The Fourier transform is performed after the full acquisition, resulting in a complete set of spectra Fig. 10 with high temporal and spectral resolution. The typical

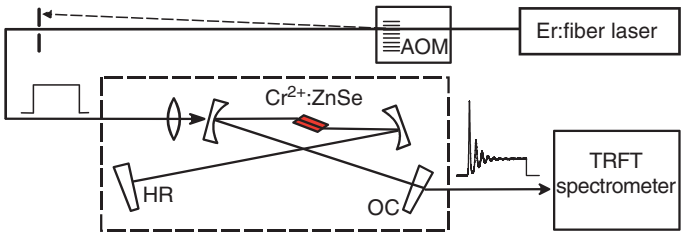

Figure 8. Schematic diagram of the time-resolved FT spectrometer. The dashed rectangle shows the evacuated chamber [21].

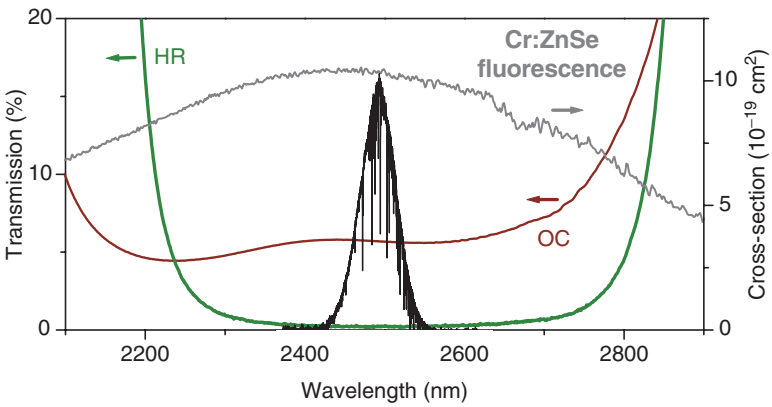

Figure 9. Fluorescence spectrum of Cr:ZnSe (gray) and spectral losses due to the output coupler (OC) and 5 high reflectors (HRs) on a round trip. A typical output spectrum at 8.9-μs delay (2.6-km effective propagation distance) is shown in black, with the CO_2 absorption lines [21].

parameters were: pulse repetition rate up to 1–3 kHz, temporal resolution 0.3–3 μs, spectral resolution 0.006–0.02 cm^{-1}.

Fig. 9 shows the laser gain curve, as well as the reflection curves of the mirrors in the cavity. One single ICLAS spectrum of CO_2 is shown, spanning over 100 nm bandwidth, at a 2.6-km effective propagation distance.

Fig. 10 shows the complete time resolved ICLAS spectrum of CO_2 at 66 mbar. Besides the CO_2, residual water lines can be seen, corresponding to contamination level of the CO_2 of about $4 \cdot 10^{-5}$ or $2.5 \cdot 10^{-3}$ mbar partial pressure of H_2O vapor.

Fig. 11 shows a high-resolution portion of the CO_2 spectrum, corresponding to 4.9 km of effective propagation distance. The effective absorption is as high as 90% for the strongest lines, corresponding to a sensitivity of 6×10^{-8} cm^{-1}. The explored spectral domain is the location of the two weak vibration-rotation combination bands $2\nu_3 - \nu_2$ (Fig. 11) and $2\nu_3 + \nu_2 - 2\nu_2$. The maximum absorption of the line profiles reaches 100% with a pressure-absorption path conditions equal to 66 mbar and 30 km, respectively. It is worth noting that previously, these spectra

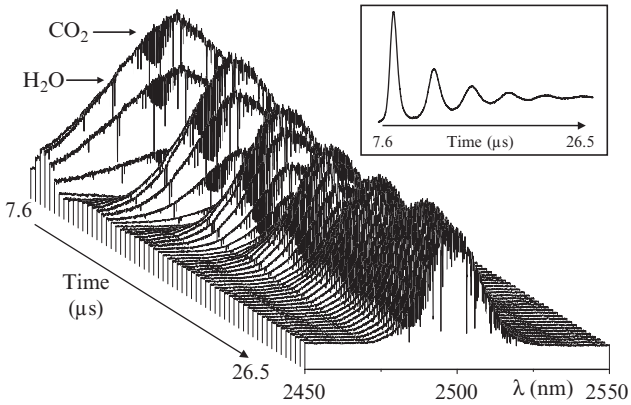

Figure 10. Time-resolved ICLAS spectrum of CO_2. The 64 consecutive time components are 0.32 μs apart. This corresponds to a 96 m increase of the equivalent absorbing path I_{eff} between each spectrum. The upper right-hand enclosure gives the total laser intensity versus time [22].

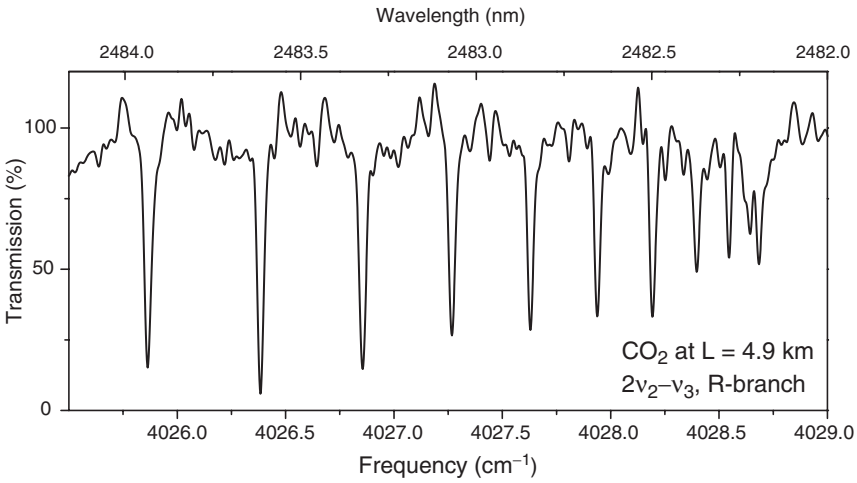

Figure 11. Doppler-limited spectrum of CO_2 at 4.9-km propagation distance [21].

could only be detected by astronomic measurements in the atmosphere of Venus [25, 26] which is 96.5% CO_2.

The sensitivity values obtained with the above setup can be further improved by reducing the intracavity losses. In particular, the output coupler can be replaced with a high reflector with transmission of the order of 0.05%. This allows longer effective path lengths and/or broader spectral coverage, according to the expression (3). The output power of the laser is of the order of few mW (from every mirror). However, since this is a diffraction-limited beam, it can be effectively delivered to the spectrometer and the signal is more than sufficient for recording the spectra. With this setup, effective path length increased up to 30

km, resulting in even higher sensitivity, reaching 10^{-8} cm^{-1} . This allowed to observe for the first time the previously unknown combination bands of acetylene C_2H_2 [27] and nitrous oxide N_2O [28] around 2.5 μm.

As already mentioned, using of the Cr:ZnS laser crystal instead of Cr:ZnSe allows shifting of the operation range of the technique by about 100 nm towards shorter waves (Fig. 7). Given the broad bandwidth of the high reflective mirrors (Fig. 9) and the fact that the Cr:ZnS crystal allows efficient pumping at 1607 nm, the experimental setup could be immediately adapted from the previous one (Fig. 8) by simple exchange of the active medium. In addition to that, the cavity length was doubled, enabling even longer effective absorption paths as described above. Fig. 12 shows a representative set of 20 Torr N_2O spectra around 2.4 μm with absorption path up to 110 km, while Fig. 13 shows a high-resolution part of the spectrum at 10.5 km effective absorption path. The broad spectrum modulation, that is seen on the long-propagation distance spectra in Fig. 12 comes most probably from the incomplete birefringence compensation in the Cr:ZnS crystal, which contains some percentage of the wurtzite phase [1]. The crystal acts in this case as a very weak Lyot filter. This modulation can be suppressed by careful orientation of the crystal or by using a material with addition of the small amount of ZnSe for cubic phase stabilization. The mixed Cr:ZnSSe crystals have shown to be good laser crystals with even broader gain bandwidth [2].

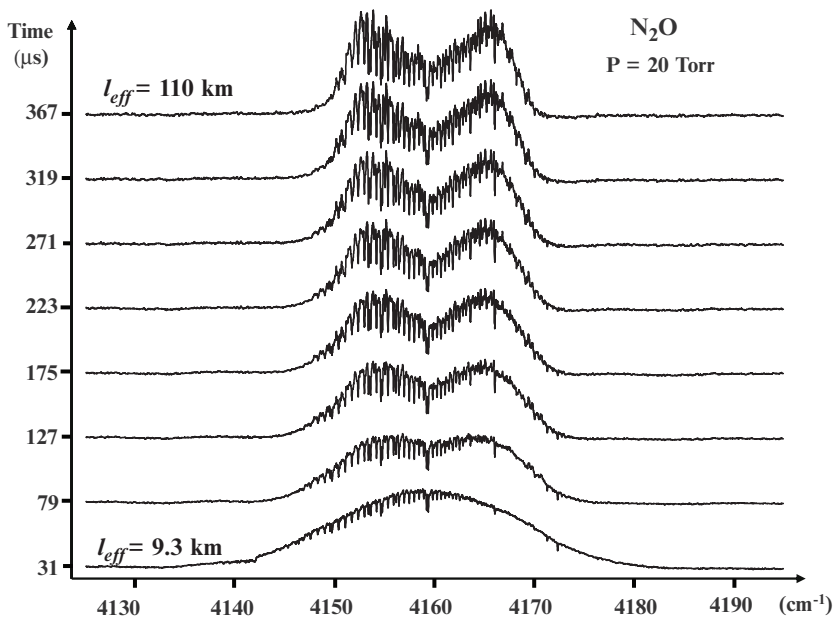

Figure 12. Intracavity absorption spectra of N_2O [29].

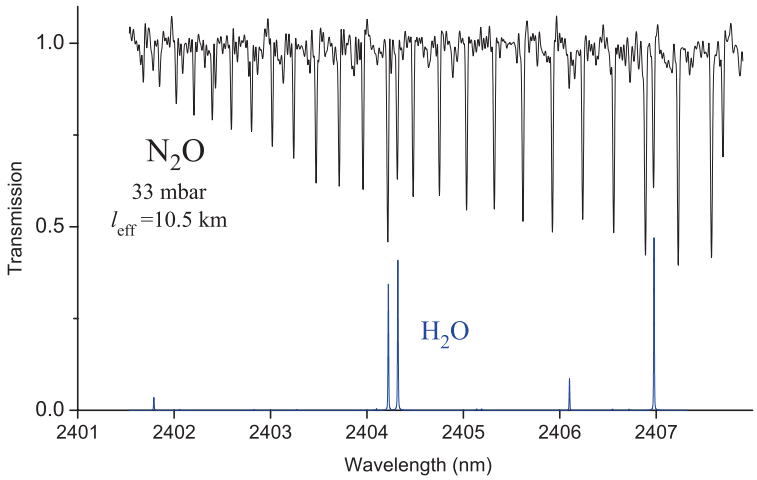

Figure 13. Intracavity absorption spectrum of N_2O at 10.5 km of absorption length. The spectral lines below show the absorption of water vapor (not to the scale). [29].

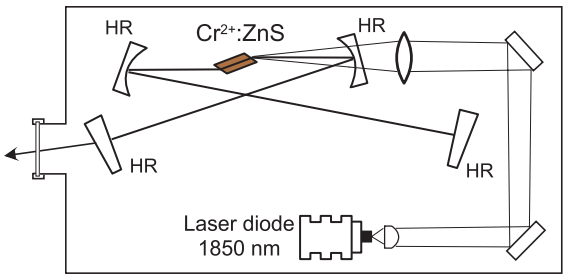

Figure 14. A self-contained sealed diode-pumped setup for intracavity absorption spectroscopy using the Cr:ZnS laser. HR: high reflector. [30].

In order to bring the mid-IR ICLAS technique closer to the applications, it should be made less complex, self-contained and user-friendly. In the case of solid-state lasers this can be achieved by direct diode-pumping. As shown in Fig. 14, the diode laser including collimation optics can be positioned inside the chamber (footprint of the laser assembly is 60 cm by 40 cm). No special light modulation is required, since the diode laser can be conveniently switched on and off with microsecond accuracy by the driving current. The price for the convenience of the diode-pumped setup is the increased pump spot in the crystal. Therefore, the laser length had to be halved with respect to the previous arrangement. The usable effective absorption path reduces correspondingly (compare Figs. 12 and 15). The estimated minimum detectable absorption (assuming signal-to-noise ratio 3 or better) is $1 \cdot 10^{-8}$ cm^{-1} versus $2 \cdot 10^{-9}$ cm^{-1} in the Er-fiber pumped system. Nevertheless, it is extremely good in comparison with other techniques in the same spectral region.

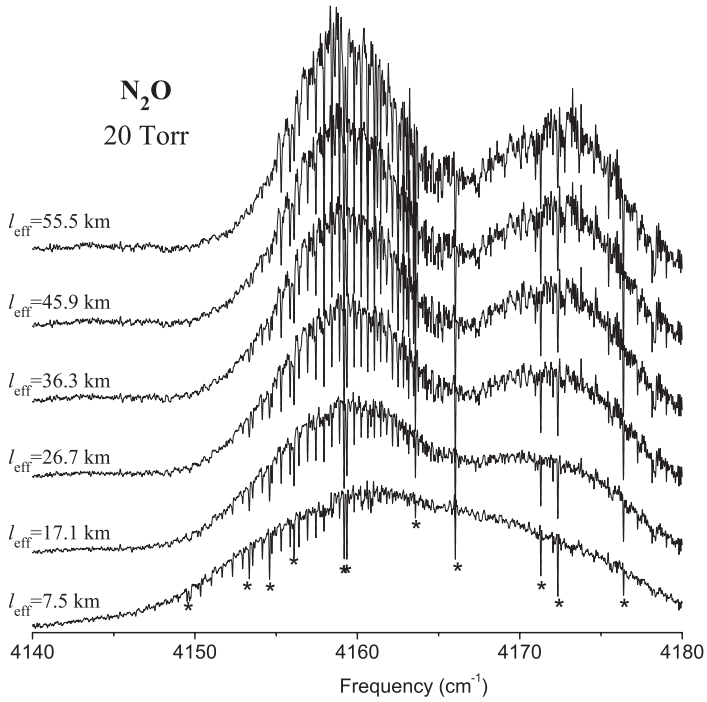

Figure 15. Intracavity absorption spectra of N_2O at different absorption lengths recorded with a diode-pumped setup. The spectral lines marked with an asterix correspond to the residual water absorption lines. [30].

5. Conclusions

The broadband mid-infrared solid-state lasers, represented by the Cr^{2+}-doped ZnSe and ZnS have come of age and are suitable for real-world applications. In praticular, detection of trace gases can be performed with extreme sensitivity and over a broad wavelength range.

In this chapter, two different approaches for spectral recordings have been demonstrated: narrowband tuning over the absorbing spectral line of interest and broadband spectrum generation using the intracavity laser spectroscopy. The registration of the absorption line in the first case has been performed using the photoacoustic technique. Obviously, any other technique, including some described in the other chapters in this book, can be applied as well. Equally, the spectrum recording by the means of Fourier-transform technique is in no way obligatory for the intracavity absorption experiments, and any other approach can be used for registration depending on the requirements of the application.

The extreme bandwidth of the solid-state lasers plays a crucial role in both demonstrated application examples. As an immediate advantage, the broad

bandwidth allows covering of a large wavelength area, thus enabling true multi-component sensitivity and selectivity using one and the same setup. In the case of intracavity spectroscopy, the broad bandwidth also translates into the highest sensitivity of the measurement, which duly reached levels of 10^{-9} cm^{-1} in terms of absorption coefficient. Such sensitivity allows recognition of gases with partial pressure of $\sim 10^{-5}$ mbar and less or recording of previously unknown very weak spectral bands.

Further improvement of both techniques are possible, and should include direct diode-pumping of the lasers in order to make them truly transportable and self-contained devices. As shown on example of intracavity measurement, this can be readily achieved with minimal trade-offs in the performance of the setup.

Acknowledgements

The experiments described in this chapter have been performed in collaboration with C. Fischer and M. Sigrist form ETH Zurich as well as with N. Picqué and G. Guelachvili form University Paris Sud, Orsay, all of whom deserve special thanks for generous sharing their expertise and equipment. I am also grateful to Dr. I. T. Sorokina from the Photonics Institute, TU Vienna, who initiated and actively participated in all the works.

The work have been supported by the Austrian National Science Fund (FWF) under grant Nr. P17973 and by the Austrian-French program Amadeus.

References

1. I. T. Sorokina: Cr^{2+}-doped II-VI materials for lasers and nonlinear optics, Optical Materials **26**, 395–412 (2004).
2. E. Sorokin, S. Naumov, I. T. Sorokina, Ultrabroadband infrared solid-state lasers, IEEE JSTQE **11**, 690–712 (2005).
3. M. Rattunde, M. T. Kelemen, N. Schulz, C. Pfahler, C. Manz, J. Schmitz, G. Kaufel J. Wagner, High-brightness $2.\times\mu$m semiconductor lasers, Chapter in this book.
4. R. Szipöcs, K. Ferencz, C. Spielmann, F. Krausz, Chirped multilayer coatings for broadband dispersion control in femtosecond lasers, Opt. Lett. **19**, 201 (1994).
5. M. W. Sigrist, ed. *Air monitoring by spectroscopic techniques. Chemical analysis series*, vol. 127. New York: Wiley; 1994 [chapter 4].
6. M. Seiter, M. W.Sigrist: Trace-gas sensor based on mid-IR difference-frequency generation in PPLN with saturated output power, Infrared Phys. Technol., **41**, 259–269 (2000).
7. A. A. Kosterev, Y. A. Bakhirkin, F. K. Tittel, Ultrasensitive gas detection by quartzenhanced photoacoustic spectroscopy in the fundamental molecular absorption bands region, Appl. Phys. B **80**, 133 (2005).
8. F. K. Tittel, D. Richter, A. Fried: *Mid-Infrared Laser Applications in Spectroscopy* in Solid-state mid-infrared laser sources, Topics Appl. Phys. vol. 89, (Springer, Berlin, 2003) pp 445–516.

9. F. K. Tittel, G. Wysocki, A. Kosterev, Yu. Bakhirkin, Semiconductor laser based trace gas sensor technology: recent advances and applications, chapter in this book.

10. E. Sorokin, *Solid-State Materials for Few-Cycle Pulse Generation and Amplification*, in Few-Cycle Laser Pulse Generation and Its Applications, Topics Appl. Phys. **95**, pp. 3–73 (Springer, Berlin, 2004)

11. C. Fischer, E. Sorokin, I. T. Sorokina, M. W. Sigrist: Photoacoustic monitoring of gases using a novel laser source tunable around 2.5 μm, Optics and Lasers in Engineering, doi:10.1016/j.optlaseng.2004.03.015.

12. E. Sorokin, I. T. Sorokina, C. Fischer, M. W. Sigrist: Widely tunable Cr^{2+}:ZnSe laser source for trace-gas sensing, paper MD4 at Adv. Solid-State Photonics 2005.

13. V. M. Baev, T. Latz, P. E. Toschek: Laser Intracavity absorption spectroscopy, Appl. Phys. B **69**, 171–202 (1999).

14. A. Kachanov, A. Charvat, F. Stoeckel, Intracavity laser spectroscopy with vibronic solid-state lasers. I. Spectrotemporal transient behavior of a Ti:sapphire laser, JOSA B **11**, 2412 (1994).

15. A. Kachanov, A. Charvat, F. Stoeckel, Intracavity laser spectroscopy with vibronic solid-state lasers: II. Influence of the nonlinear mode coupling on the maximum sensitivity of a Ti:sapphire laser, JOSA B **12**, 970 (1995).

16. V. M. Baev, V. P. Dubov, A. N. Kireev, E. A. Sviridenkov, D. D. Toptygin, O. I. Yushchuk, Application of lasers with Fa(II) color centers in KCl:Li crystals in intracavity laser spectroscopy, Sov. J. Quantum Electron. **16**, 1121–1123 (1986).

17. M. P. Frolov, Yu. P. Podmar'kov: Intracavity laser spectroscopy with a Co:MgF_2 laser, Opt. Comm. 155, 313–316 (1998).

18. A. Stark, L. Correia, M. Teichmann, S. Salewski, C. Larsen, V. M. Baev, P. E. Toschek: Intracavity absorption spectroscopy with thulium-doped fibre laser, Opt. Comm. 215, 113–123 (2003).

19. V. A. Akimov, V. I. Kozlovsky, Yu. V. Korostelin, A. I. Landman, Yu. P. Podmar'kov, M. P. Frolov, Intracavity laser spectroscopy using a Cr^{2+}:ZnSe laser, Quantum Electron. **34**, 185–188 (2004).

20. F. Gueye, E. Safari, M. Chenevier, G. Guelachvili, N. Picqué, Intracavity Cr^{4+}:YAG laser absorption analyzed by time-resolved Fourier transforms pectroscopy, Appl. Phys. B **81**, 1143 (2005).

21. E. Sorokin, I. T. Sorokina, N. Picqué, F. Gueye, G. Guelachvili, Mid-IR High-Resolution Intracavity Cr^{2+}:ZnSe Laser-Based Spectrometer, paper MD3 at Adv. Solid-State Photonics 2005.

22. N. Picqué, F. Gueye, G. Guelashvili, E. Sorokin, I. T. Sorokina, Time-resolved Fourier transform intracavity spectroscopy with a Cr^{2+}:ZnSe laser, Opt. Lett., **30**, 3410 (2005).

23. E. Sorokin, I. T. Sorokina, G. Guelachvili, M. Jacquemet, N. Picqué, Diode-pumped mid-IR Cr^{2+}:ZnS-laser-based spectrometer, paper SyB4 at 2nd EPS-QEOD Europhoton Conference, Pisa, Sept. 10–15, (2006).

24. N. Picqué, G. Guelachvili: High-information time-resolved Fourier transform spectroscopy at work, Appl. Opt. **39**, 3984–3990, 2000.

25. P. Connes, G. Michel, High-resolution Fourier spectra of stars and planets, Astrophysical Journal. Letters to the Editor **190**, L29-32 (1974).

26. J.-Y. Mandin, Interpretation of the CO_2 absorption bands observed in the Venus infrared spectrum between 1 and 2.5 μm, J. Mol. Spectrosc. **67**, 304–321 (1977).

27. V. Girard, R. Farrenq, E. Sorokin, I. T. Sorokina, G. Guelachvili, N. Picqué, Acetylene weak band spectroscopy at 2.5 μm from time-resolved Fourier transform intracavity Cr^{2+}:ZnSe laser absorption, Chem. Phys. Lett. **419**, 584 (2006).

28. H. Herbin, N. Picqué, G. Guelachvili, E. Sorokin, I. T. Sorokina, N_2O weak lines observed between 3900 and 4050 cm^{-1} from long path absorption spectra, J. Mol. Spectroscopy **238**, 256 (2006)

29. E. Sorokin, I. T. Sorokina, G. Guelachvili, M. Jacquemet, N. Picqué, Sensitive Broadband Mid-IR Cr^{2+}:ZnS-Laser-Based Spectrometer, CLEO/QELS May 21-26, Long Beach, CA, USA, Technical Digest on CD, paper CFL5 (2006).

30. E. Sorokin, I. T. Sorokina, G. Guelachvili, M. Jacquemet, N. Picqué, Diode-pumped mid-IR Cr^{2+}:ZnS-laser-based spectrometer, paper SyB4 at 2nd EPS-QEOD Europhoton Conference, Pisa, Sept. 10-15, (2006).